A Thermal Habitat for RNA Amplification and Accumulation

Annalena Salditt[a#], Lorenz M. R. Keil[a#], David P. Horning[b#],

Christof B. Mast[a], Gerald F. Joyce[b] & Dieter Braun[a*]

Affiliations: [a]Systems Biophysics, Physics Department, Center for Nanoscience, Ludwig-Maximilians-Universität München, 80799 Munich, Germany
[b]The Salk Institute, 10010 N. Torrey Pines Road, La Jolla, CA 92037
* Corresponding author. Email: dieter.braun@lmu.de; Phone: +49-89-2180-1484
# Contributed equally

Supplementary Methods

Finite-element simulations

The finite-element simulations are performed in an axi-symmetric compartment with rectangular cross section using Comsol Multiphysics 5.4. The simulation file with all the detailed parameters is given in the supplement in binary format. Additionally, the simulation is given as human-readable auto-generated report in a hierarchical html compressed into a Zip-File.

A punctual heat source in the cylindrical compartment forms a temperature gradient, pointing outward from the given heat spot. The temperature profile was measured by the temperature dependent fluorescence decrease of BCECF as described in the materials section. This temperature measurement averages over the height of the chamber. In order to model the experimental situation correctly, we have implemented a corresponding height average of the 2D temperature calculation in Comsol and adjusted the modelled heating power and beam width of the laser so that numerical and experimental temperature profiles matched within 20 %and 30 % error, respectively.

Using the axisymmetric nature of the experimental setting, the following partial differential equations could be reduced to 2D which increases computing speed and still allows to fully model the three-dimensional experiment. The experimentally validated temperature profiles were fed into the numerical model which couples the contributing transport mechanisms as described below:

(i) The temperature profile is calculated by using partial differential equations for transient heat transfer with the material parameters of water, silicon, silicone and glass. For water, the temperature dependence of all contributing parameters was fully considered. The Absorption of the Gaussian shaped IR laser is modeled based on Beer-Lambert law and the photon momentum upon absorption is considered in the force balance of the Navier-Stokes equation since this can slow down convection by up to 30 %. The absorption coefficient for the IR light of 1940 nm is given by 129.6 1/cm according to published materials constants.

(ii) The numerical solution of the incompressible Navier-Stokes equation derives the convective flow profile inside the thermal convection chamber. The temperature-dependent density is used to calculate the buoyancy force. Non-slip boundary conditions and a zero-pressure point boundary are used. The enhanced viscosity of the rPCR buffer due to the addition of PEG is experimentally measured via Brownian motion of fluorescently labeled, 1 µm sized, beads. At a temperature of 20 °C, the viscosity is given by 28 mPas×s.

(iii) The accumulation of the 35mer, 210mer and PEG8000 are solved by a convection-diffusion equation that is solved using the simulated flow and temperature profile. The thermophoresis and diffusiophoresis are implemented by a molecular flow, counterbalanced by the diffusion along a concentration difference. Boundaries are given as non-adsorbing boundaries. The molecular flux $\vec{J_i}$

for a nucleic acid species i is defined by diffusion, thermophoresis, and convection. It can be described by

$$\vec{J_i} = -D_i \nabla c_i - S_{Ti} D_i \nabla T c_i + \vec{v} c_i \qquad \text{(S1)}$$

where c_i, D_i, S_{Ti} and $\vec{v}$ denote the concentration of molecule, diffusion, Soret coefficient and convective transport. The Soret coefficients for the 35mer and the 210mer are given by 0.03 K^{-1} and 0.2 K^{-1}, respectively, which is about a factor of 3 higher than what is expected from literature values with different salts at a comparable Debye length. The deviations are however, expected for PEG-mixtures with high concentrations of $MgCl_2$ and the 0.9 M TPA because the Seebeck effect dominates thermophoresis in this regime and many of the electrophoretic mobilities which determine the buildup of the electric field are not known. Therefore, changing the Soret coefficients within this range appears to be a realistic approach.

The Soret coefficient of the RNA polymerase conglomerates were assumed to be 0.3 K^{-1}, thus only slightly higher than the Soret coefficient for the 210mer. However, it should be noted that the diffusiophoretic forces are dominating the ring formation and thermophoresis is a rather minor effect. The diffusion coefficients are adapted from Mast *et al*[1]. following $D = 0.5 \cdot 643 \cdot n_i^{-0.46} \cdot D_{PEG_{factor}} D_{Viscosity\_fac}$ for dsRNA in salty conditions, where n denotes the length of the strand. With $D_{PEG_{factor}}$ we have modelled the slower diffusion brought about by the enhanced viscosity of a thermophoretically enhanced PEG concentration. To fully model the interaction between the concentration profile of PEG8000 and the nucleic acid conglomerates, the total flux was extended by diffusiophoretic terms to

$$\vec{J_i} = -D_i \nabla c_i - S_{Ti} D_i \nabla T c_i + (\vec{v} + \vec{u}) c_i \qquad \text{(S2)}$$

following[2], where the additional interaction is described by the diffusiophoretic velocity $\vec{u}$ of DNA, given by

$$\vec{u} = \frac{0.5 \cdot k_B T}{3\eta/\mu} \cdot \left(S_{T_{PEG}} - \frac{1}{T}\right) \cdot r_{G_{PEG}}^2 \frac{N_A c_i c_{0_{PEG}}}{c_{0i}}. \qquad \text{(S3)}$$

Here, $r_{G_{PEG}}$ is the radius of gyration of PEG8000, η/μ is the corrected viscosity and $c_{0_{PEG}}$ is the initial concentration of PEG. It should be noted that the temperature dependence of the viscosity of the PEG-water mixture was assumed to be similar to the temperature dependence of the viscosity of pure water, while being corrected by a factor of 7.3 that was experimentally obtained at 17 °C.

Random walk model

Random walk simulations are used to derive statistical data on thermal cycles of RNA oligonucleotides inside the thermal habitat. The temperature cycle statistics consider the movement of 400 particles for 2 h time frame, given time-steps of $\Delta t = 1ms$. The displacement of particles is thereby given by

$$\Delta\vec{s}(x,y) = \sqrt{4 \cdot D \cdot \Delta t} \cdot \vec{\eta}(t) + \Delta t \cdot (\vec{v}(x,y) + D \cdot S_T \cdot \nabla T(x,y)) \quad \text{(S4)}$$

where Δt denotes the time-step, T the local temperatures, and $\vec{v}(x,y)$ the flow profile of the respective species that was calculated beforehand by finite element simulations (see chapter finite-element simulations). Brownian motion is implemented by a randomly directed movement $\vec{\eta}(t)$. Molecules complete a full temperature cycle when moving from a high temperature region (>60 °C for denaturation) to a low temperature region (<20 °C for elongation) and back to a high temperature region. The minor change in molecule size during the experiment due to partial elongation scenarios by the polymerase is, however, not considered in the random walk model.

Sigmoidal model for exponential replication

The exponential replication of RNA can be described theoretically by a sigmoidal model[3], where the product concentration c is dependent on the number of cycles according to:

$$c(cycle) = \frac{c_{max}}{1+e^{-(cycle-cycle_{1/2})/k}}, \quad \text{(S5)}$$

where c_{max} denotes the final maximal concentration, k the replication factor, $cycle$ the number of cycles and $cycle_{1/2}$ cycle factor corresponding to the midpoint of the growth curve and is given by

$$cycle_{1/2} = k \cdot ln(\frac{c_{max}}{c_0} - 1) \quad \text{(S6)}$$

. This model starts with an initial exponential growth phase for $c \ll c_{max}$. Later, the replication is inhibited, which can be attributed to a depletion of primers and NTPs, a decline in polymerase ribozyme activity and the presence of pyrophosphates. In the experiment, the number of cycles is held fix at 50. Therefore, the dependence of the final concentration c_{max} on the initial template concentration c_0 which is used to fit the results in Figure 2b is given by:

$$c_{50}(c_0) = \frac{c_{max}}{1+e^{(ln(\frac{c_{max}}{c_0}-1)-\frac{cycle}{k})}} \quad \text{(S7)}$$

The replication efficiency E describes the increase of the concentration c between two consecutive cycles $cycle_N$ and $cycle_{N-1}$ given by $E = c_N/c_{N-1}$. For the initial exponential phase ($c \ll c_{max}$) the expression for E simplifies to $E = e^{1/k}$, which was used to calculate the stated values for convection and bulk, respectively.

Prediction of RNA cleavage rates

The rates of RNA degradation due to transesterification can be predicted following Li and Breaker[4] with

$$k_{degrad} = k_{bg} \cdot 10^{0.983(pH-6)} \cdot 10^{-0.24(3.16-[K+])} \cdot 69.3 \cdot [Mg2+]^{0.80} \cdot 3.57[K+]^{-0.419} \cdot 10^{0.07(T1-23)}, \qquad \text{(S8)}$$

where $k_{bg} = 1.3 \cdot 10^{-9}$ min^{-1} is the background rate for pH 6 , $[K+] = 3.16$ M and at 23 °C. The experimental values of $[Mg2+] = 0.05$ M, $[K+] = 0.05$ M and pH 8.3 were assumed to be stationary. This temperature dependent degradation rate was included as additional term in the modified convection-diffusion equation, leading to:

$$\nabla(-D_i \nabla c_i - S_{Ti} D_i \nabla T c_i + (\vec{v} + \vec{u}) c_i) = R_i, \qquad \text{(S9)}$$

with $R_i = -c_i \cdot k_{degrad}$. To investigate whether the phoretic transports lead to a protection from degradation, the simulation was run for the case described in (S9), as well as for an artificial case without any phoretic forces, following:

$$\nabla(-D_i \nabla c_i + \vec{v} c_i) = R_i. \qquad \text{(S10)}$$

For both cases, surface integral over the resulting concentration was performed to evaluate the total remaining concentration at each time point.

Supplementary Tables

Sequences of RNA molecules
Both primers pose a 5'-tag to improve the polymerase ribozyme processivity and a FAM modification.

Type	RNA Sequence (5'-3')
Fwd. Primer	GACAAUGAC AAAAAA GCAACUUUUC
Rev. Primer	GACAAUGAC AAAAAA CACUCCACAC
rPCR Template	GACAAUGAC AAAAAA CACUCCACAC GAAAAGUUGC
24-3 Polymerase	AGU CAU UGC CGC ACG AAA GAC AAA UCU GCC CUC AGA GCU UGA GAA CAU CUU CGG AUG CAG AGG AGG CAG CCU UCG GUG GAA CGA UCG UGC CAC CGU UCU CAA CAC GUA CCC GAA CGA AAA AGA CCU GAC AAA AAG GCG UUG UUA GAC ACG CCC AGG UGC CAU ACC CAA CAC AUG GCU GAC
dsDNA	TCG GTG TAG GTC GTT CGC TCC AAG CTG GGC TGT GTG CAC GAA CCC CCC GTT CAG CCC GAC CGC TGC GCC TTA TCC GGT AAC TAT CGT CTT GAG TCC AAC CCG GTA AGA CAC GAC TTA TCG CCA CTG GCA GCA GCC ACT GGT AAC AGG ATT AGC AGA GCG AGG TAT GTA GGC GGT GCT ACA GAG TTC TTG AAG TGG TGG CCT AAC TAC GGC

Supplementary Table 1 | RNA sequences for the ribozymatic replication of RNA (top). For the accumulation experiments, the template sequence, the 24-3 polymerase and its sequence analog were used. The 210nt long dsDNA was amplified from the pBR322 plasmid via a standard PCR.

Supplementary Figures

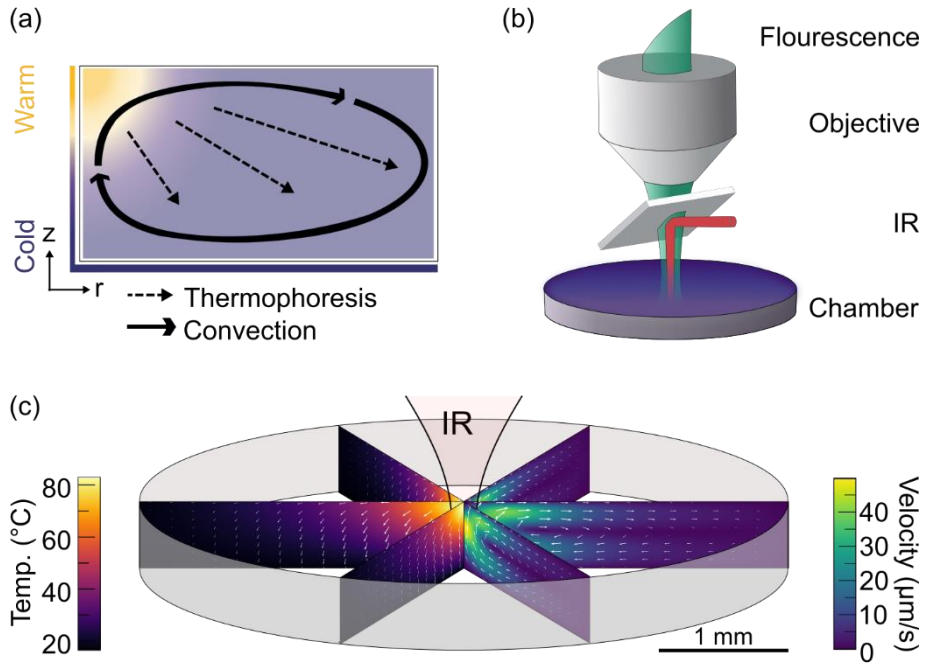

Supplementary Figure 1 | Thermally driven convective habitat. (a) A temperature gradient induces two effects in solution, thermophoresis and convection. For a punctual heat source the resulting convection exhibits temperature characteristics of extended periods at cold temperatures and short temperature spikes. The superposition of both effects results in an efficient length dependent accumulation mechanism for polymers. These characteristics can be found for a fully cylindrical compartment as well as partially revolved compartments. (b) A radial symmetric heat profile is applied using a focused IR-Laser that mimics a naturally heated pore. The accumulation kinetics are observed using a fluorescence microscope. (c) The absorption of an IR laser in the upper layers of a cylindrical compartment induces a convective motion of the fluid. The white arrows in the temperature profile and velocity profile indicate the thermophoretic and convective velocity, respectively. Note, that the length of the arrows is scaled for better visibility and does only reflect the relative strengths of the respective velocity fields.

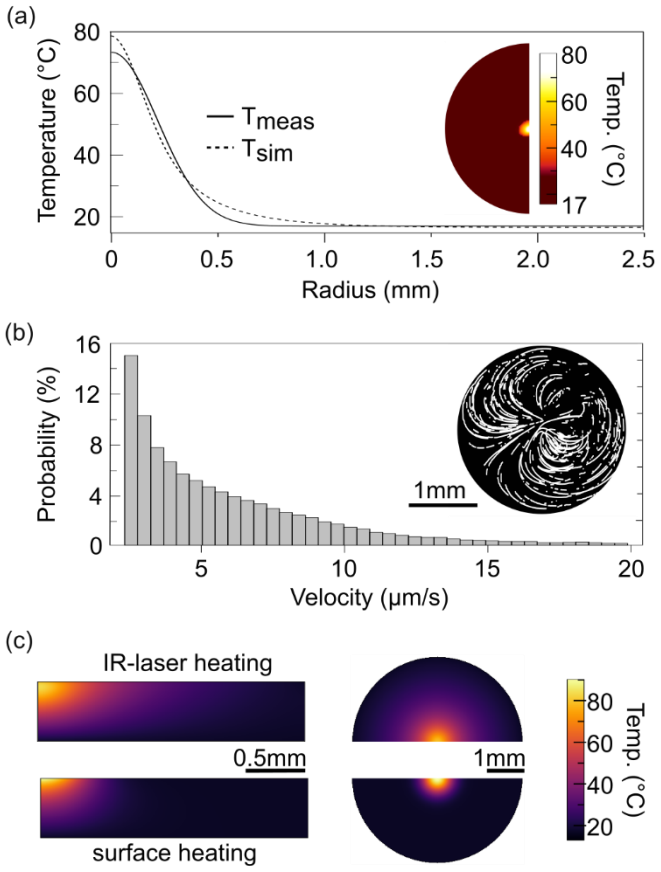

Supplementary Figure 2 | IR laser induces convective motion of macromolecules. (a) The Gaussian profile of the IR laser locally heats the compartment in the center. Here, the laser induces a temperature difference between heated regions (80 °C) and the bottom layer, which is actively cooled to 17 °C. The radial temperature profile is derived from the temperature dependent fluorescence of BCECF (50 µM) diluted in TRIS buffer (10 mM). Experimentally derived temperatures are in good agreement with a 3D finite-element simulation, using the axial symmetry of the system. (b) The temperature gradient induces a convective flow which shuttles 1 µm sized, fluorescently labeled beads between the inner and outer parts of the chamber. In the majority of time, the molecules (or beads in this case) are in regions with low velocities and only spend short amount of times at the central region with high velocities. The maximum velocities of above 20 µm/s occur in the heated regions of the chamber. (c) Finite-element simulations showed that similar temperature profiles can be achieved by heating the compartment with an IR-laser or by heating the surface.

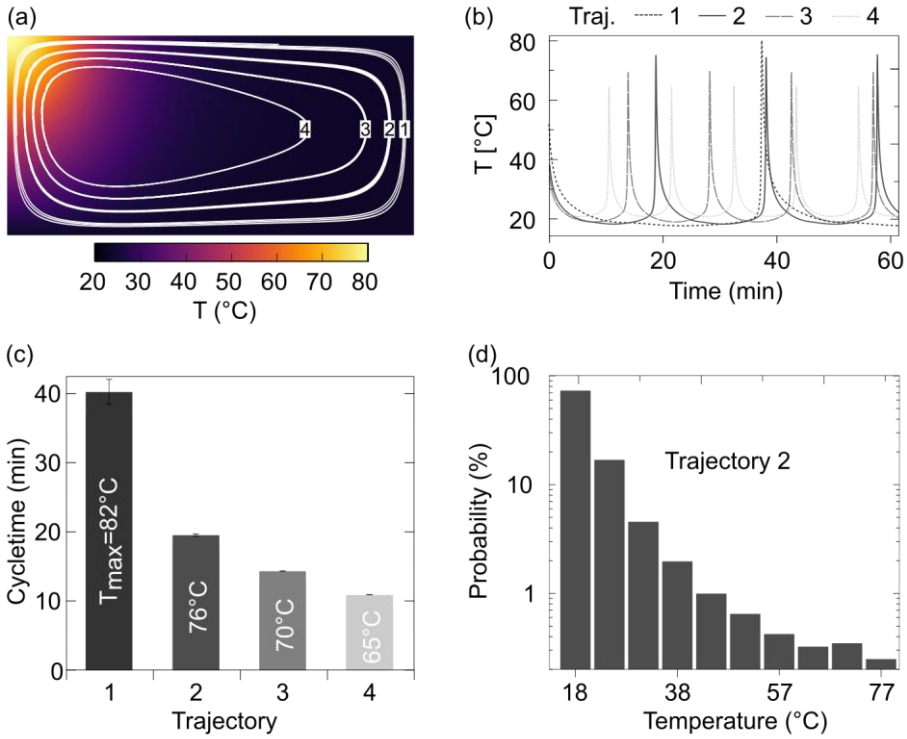

Supplementary Figure 3 | Finite-element simulation derived temperature cycle conditions. (a) Exemplary trajectories of macro molecules solely driven by thermal convection. Various thermal scenarios were screened to find a scenario that matches the delicate temperature conditions necessary for RNA amplification. For this purpose, a finite-element simulation derives temperature cycles of molecules with respect to its initial starting position, neglecting thermophoretic and Brownian motion. (b) The temperature oscillation inside a chamber of 0.5 mm in height and 2.25 mm radius matches the temperature cycle requirement of a RNA-only replication system. Here, molecules undergo fast temperatures changes while remaining for most of the time at low temperatures. (c) Simulating 400 trajectories of random starting positions yield a mean cycle time of 19.0±10.3 min between 20 °C and 60 °C. More excessive temperature oscillations, such as temperature differences between 20 °C and 80 °C, require extended cycle times of 55.8±18.0 min. (d) In these thermal habitats, the molecules are convectively shuttled between regions of varying temperatures, however remain at low temperatures for most of the time.

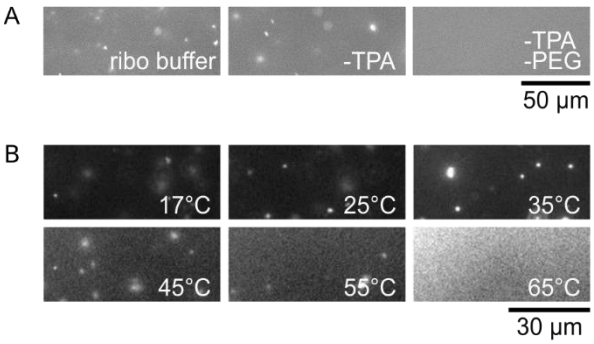

Supplementary Figure 4 | Characteristics of nucleic acids conglomerates exemplary shown for RNA. (a) Successively removing individual buffer components revealed that PEG8000 is crucial component driving the formation of conglomerates. (b) Additionally, the conglomerates exhibit a temperature dependence, where they reversibly disappear and reemerge at higher and lower temperatures, respectively.

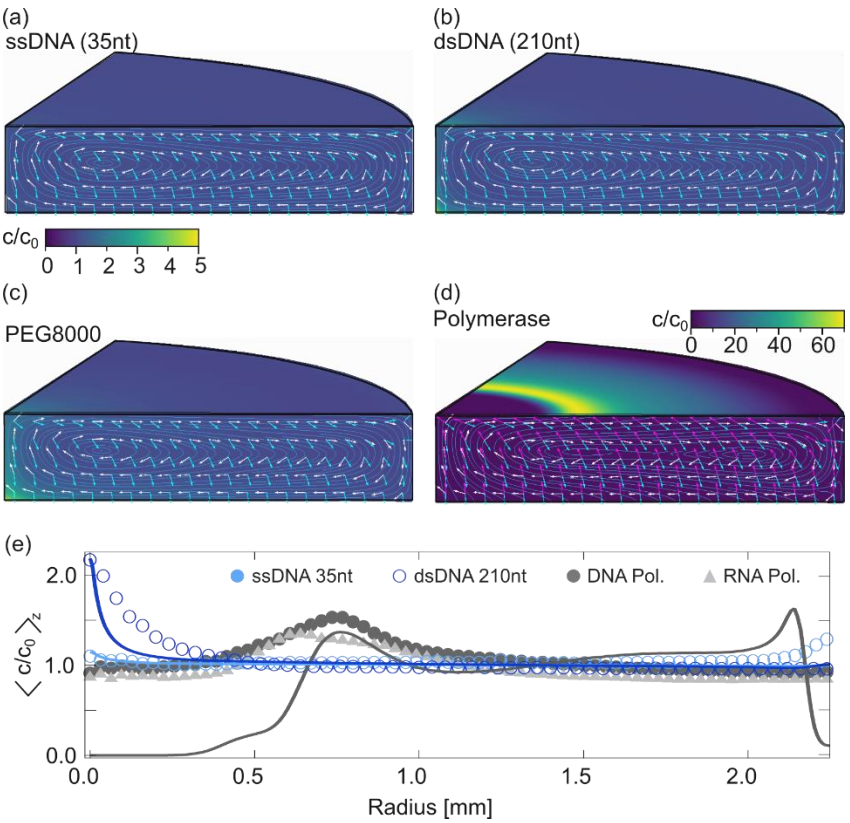

Supplementary Figure 5 | Accumulation profiles derived by finite-element simulations. The white, cyan and magenta arrows represent the normalized direction of the convective, thermophoretic and diffusiophoretic movement, respectively. Note, that the length of the arrows is scaled for better visibility and only serves as indicator of the respective directions for the various velocity profiles. The streamlines, indicated in light blue, correspond to the superposition of all velocity profiles. (a) The ssDNA of 35nt length exhibits a 1.33-fold concentration increase after 60 min and thus has an almost negligible accumulation. (b) The dsDNA of 210nt length shows a clear accumulation with a 5-fold concentration increase after 60 min at the bottom center of the compartment. (c) Simulating the accumulation behavior of PEG8000 inside the convection chamber reveals that PEG exhibits a similar behavior as the 210mer. The maximum concentration increase after 60 min is 4.5-fold, again at the bottom center of the compartment. The concentrations for the ssDNA, dsDNA and PEG are scaled to a 5-fold concentration increase for better comparability. (d) Only for the slow diffusing conglomerates, diffusiophoresis becomes a significant driving force and is opposing the thermophoretic driving. After 60 min the initial concentration shows a maximum of 66-fold increase in a ring-shaped geometry. The streamlines reveal the molecular movement towards the wall in the ring shaped accumulation. (e) Radial and height averages were used to match the simulation with the experimental fluorescence data. The height average $\langle c/c_0 \rangle_z$ of the simulated concentrations (lines) reproduced the experimental fluorescence signal (symbols) for all species. Data points represent the radially averaged and background corrected fluorescence intensities.

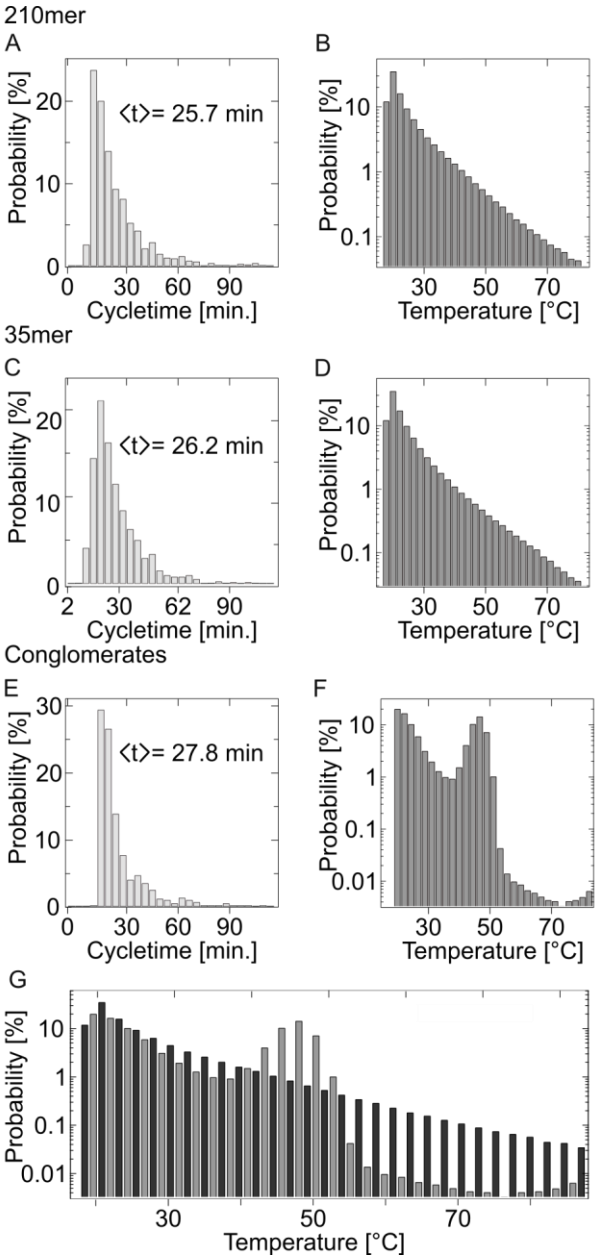

Supplementary Figure 6 | Cycling and temperature characteristics derived from stochastic trajectories. The statistics are obtained from a total of 400 simulated trajectories corresponding to a total time span of 2 h. (a), (b) and (c), (d) show the distributions of cycling times and temperatures for the 210nt long dsDNA and the 35nt long ssDNA, respectively. A cycle corresponds to a trajectory that starts T<20 °C moved to T>60 °C and back to T<20 °C. The strands mainly remain at low temperatures and only quickly cycle through high temperature spots. (e) Random walk simulations for the conglomerates yield no trajectories that complete the full temperature cycle with a spike temperature of above 60 °C. Here, the cycling times correspond to trajectories between T<20 °C and T>40 °C. (f) The temperature distribution shows a second peaks around 45 °C corresponding to the temperature at the accumulation. (g) Although the conglomerates have a higher residence probability at temperatures around 45 °C compared to the 35mer, the probability drops for temperatures above 60 °C.

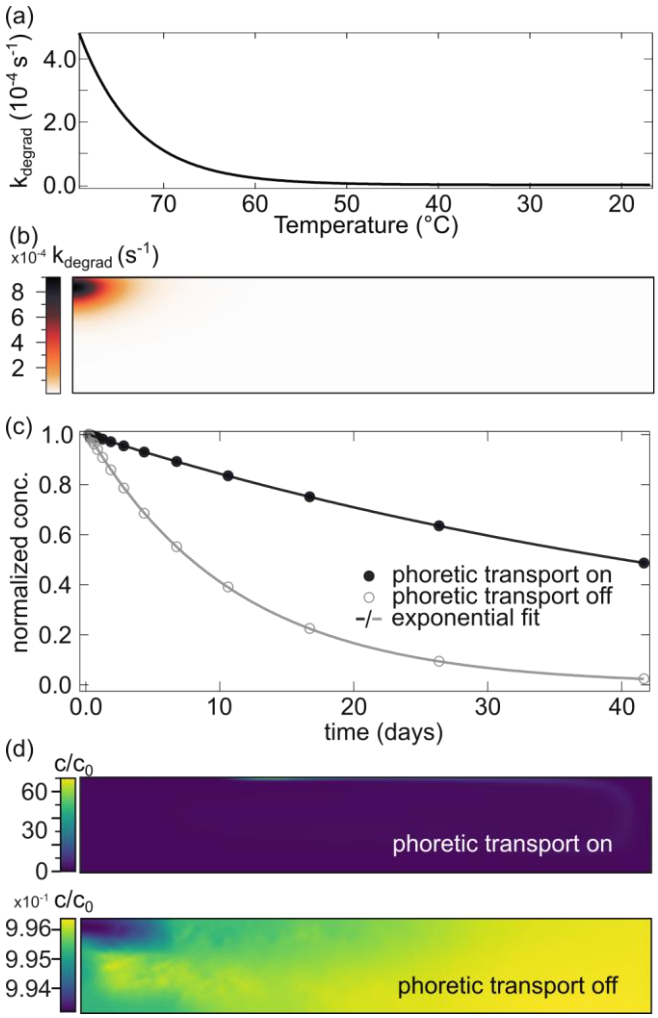

Supplementary Figure 7 | Simulation results for the effect of the temperature dependent RNA cleavage on the concentration of the polymerase. (a) The rate for RNA cleavage was implemented in the finite element simulation as described in the SI methods. As expected it shows a strong temperature dependence, with a minimal rate of $k_{degrad} = 2.13 \cdot 10^{-8}$ s^{-1} at 17 °C and a maximal rate of $k_{degrad} = 9.19 \cdot 10^{-4}$ s^{-1} at 83.2 °C, respectively. Although the actual values have to be taken with caution the relative trend of the rate should be reliable. (b) depicts the linear representation of the RNA cleavage rate in the 2D axisymmetric compartment. (c) In both cases we found an exponential degradation of the (surface averaged) ribozyme. Fitting an effective degradation rate, a more than 5-fold more stable ribozyme degradation rate was found for the case of accumulation. This is due to the phoretic transports, that are accumulating the ribozyme conglomerates to colder areas in the chamber. For long time scales, relevant in the emergence of live this might have played the essential role for selection pressure towards more structured molecules. (d) The concentration profile for both cases, with and without phoretic transport are shown for t=60 min. The difference of maximal accumulation compared to a scenario without degradation negligible. As expected the concentration profile for the case without phoretic transport shows no accumulation and only small differences in absolute values for the concentration. However, a significant fraction of the polymerase is constantly exposed to very high temperatures, resulting in a higher effective cleavage rate.

Supplementary Movies

M1 | Supplementary Movie 1
Accumulation of ssDNA (35nt), dsDNA (210nt), RNA polymerase and its sequence analog inside a thermal convection chamber. The thermal habitat is experimentally mimicked a punctual heat source using an IR-laser that applies a radial symmetric heat profile across a cylindrical shaped compartment. Here, the 210mer oligonucleotides accumulated beneath the heated regions, whereas the RNA polymerase and its DNA analog show a ring-shaped concentration increase. The 35mer shows no significant accumulation.

M2 | Supplementary Movie 2
Qualitative visualization of µm-sized particles in the convection chamber. The polystyrene beads with a diameter of 1 µm are transported by the convective flow between inner and outer regions of the chamber. As a result, the convective motion shuttles the molecules between regions of varying temperature, prompting them to undergo subsequent temperature cycles. The bead movement is observed under a fluorescence microscope over the course of 22 min.

M3 | Supplementary Movie 3
Temperature dependence of the conglomerates formed by the RNA polymerase and its sequence analog. Both, DNA and RNA form conglomerates at temperatures < 17 °C. By gradually increasing the temperatures to 45-50 °C, the conglomerates disappear and only reemerge after cooling down the solution.

References

1. Mast, C. B., Schink, S., Gerland, U. & Braun, D. Escalation of polymerization in a thermal gradient. *Proc. Natl. Acad. Sci.* **110**, 8030–8035 (2013).
2. Maeda, Y. T., Tlusty, T. & Libchaber, A. Effects of long DNA folding and small RNA stem-loop in thermophoresis. *Proc. Natl. Acad. Sci.* **109**, 17972–17977 (2012).
3. Swillens, S., Dessars, B. & Housni, H. El. Revisiting the sigmoidal curve fitting applied to quantitative real-time PCR data. *Anal. Biochem.* **373**, 370–376 (2008).
4. Li, Y. & Breaker, R. R. Kinetics of RNA degradation by specific base catalysis of transesterification involving the 2γ-hydroxyl group. *J. Am. Chem. Soc.* **121**, 5364–5372 (1999).